Ihnatiuk, D.; Vorobets, V.; Šihor, M.; Tossi, C.; Kolbasov, G.; Smirnova, N.; Tittonen, I.; Eremenko, A.; Kočí, K.; Linnik, O.

Photoelectrochemical, photocatalytic and electrocatalytic behavior of titania films modified by nitrogen and platinum species

Published in:
Applied Nanoscience (Switzerland)

DOI:
10.1007/s13204-021-01690-1

Published: 01/03/2022

Document Version
Publisher's PDF, also known as Version of record

Applied Nanoscience
https://doi.org/10.1007/s13204-021-01690-1

ORIGINAL ARTICLE

Photoelectrochemical, photocatalytic and electrocatalytic behavior of titania films modified by nitrogen and platinum species

D. Ihnatiuk[1] · V. Vorobets[2] · M. Šihor[3] · C. Tossi[1] · G. Kolbasov[2] · N. Smirnova[4] · I. Tittonen[1] · A. Eremenko[4] · K. Kočí[3] · O. Linnik[4]

Received: 26 December 2020 / Accepted: 19 January 2021

Abstract

Co-doping of titania by N and Pt species was employed to tune the electronic structure and enhance the electrocatalytic and photocatalytic activity of the films. Herein, the different approaches of synthesis procedure of Pt- and Pt,N–TiO_2 films were used to investigate their effect on the platinum oxidation states. The resulting different species of Pt led to the changes in the electronic structure of TiO_2, with consequent bandgap narrowing, anodic shift of the flat band potential, and cathodic shift of the valence band The quantum yield efficiency was correlated with Pt^0 atomic content and the relative atomic content of Pt^{n+}–O–Ti fragments, whereas its decrease for some samples can be caused by the presence of N and Pt^{n+}. The highest response for N_2O photocatalytic decomposition was observed over Pt,N–TiO_2 films. The presence of metal and non-metal species in TiO_2 structure resulted in synergistic effect including (1) inhibition of recombination of the electrons and holes and (2) narrowing of the bandgap. Electrocatalytic properties in hydrogen and oxygen evolution reactions were improved by Pt doping. The formed Pt^{2+}–O–Ti bonds rather than Pt nanoparticles are suggested to be responsible for the highest electrocatalytic activity. The additional UV exposure of the electrodes led to Pt NPs aggregation as a result of photodeposition of Pt ions. The mechanism of the Pt^{2+} photoreduction in TiO_2 structure is proposed.

Keywords Nitrogen incorporation · Titania films · Pt ions · Photocatalytic N_2O decomposition · Electrocatalytic oxygen and hydrogen evolution

Introduction

Overcoming the problems related to global warming, environmental pollution and energy crisis requires modern technologies based on the catalytic and photocatalytic processes, such as organic and inorganic pollutants degradation, photocatalytic and catalytic CO_2 and N_2O decomposition, electrochemical–photoelectrochemical evolution of oxygen and hydrogen (Dolat et al. 2013; Gaidai et al. 2017; Goncharuk et al. 2019; Khalyavka et al. 2019; Ischenko et al. 2008; Linnik et al. 2009; Reli et al. 2017).

N_2O is recognized as a greenhouse gas responsible for global warming. Despite it only comprising 320 ppb of the Earth's atmosphere, its contribution to global warming is important. N_2O has a GWP100 (global warming potential time horizon of 100 years), which is nearly 300 times higher than that of CO_2 (Richter and Caillol 2011). N_2O photocatalytic decomposition under UV irradiation in presence of a photocatalyst is one of the prospective methods for its removal. The UV active photocatalyst used as a worldwide standard—TiO_2—has been widely tested for N_2O photocatalytic decomposition (Kočí et al. 2012; Obalova et al. 2013; Sano et al. 2000): ecologically friendly in the form of powders, coatings and films, it remains the most studied and promising semiconductors for these processes in the

✉ O. Linnik
okslinnik@yahoo.co.uk

1 Micro and Quantum System Group, Department of Electronics and Nanoengineering, Aalto-University, Tietotie, 3, 02150 Espoo, Finland

2 Institute of General and Inorganic Chemistry of National Academy of Sciences of Ukraine, Acad. Palladin Str. 32/34, Kyiv 03680, Ukraine

3 Institute of Environmental Technology, CEET, VSB - Technical University of Ostrava, 17. listopadu 2172/15, Ostrava-Poruba 708 00, Czech Republic

4 Chuiko Institute of Surface Chemistry of National Academy of Sciences of Ukraine, General Naumov Str. 17, Kyiv 03164, Ukraine

Published online: 08 February 2021

last decades (Etacheri et al. 2015; Ismail et al. 2010; Kisch 2015; Rothenberger et al. 1992). Nowadays, the emphasis is on TiO_2 sensitization to the visible light and optimization of interfacial charge–transfer reactions via doping with non-metals, metal ions, narrow-gap semiconductors, noble metal nanoparticles and metal oxides (Beranek and Kisch 2008; Choi et al. 2010; Etacheri et al. 2015; Linnik et al. 2020; Tossi et al. 2019). Titania modification with metals' ions leads to the change in the electronic structure, particle size and specific surface area, effecting the photocatalytic activity as a result of higher efficiency for the electron–hole generation, the charge trapping and enhanced interfacial charge–transfer (Smirnova et al. 2017, 2019; Singh et al. 2008). Titania co-doping by nitrogen and metal ions is expected to improve the photocatalytic response for both UV and visible light resulting in effective photocatalytic processes. However, stimulated absorption under low energy light and efficient charge separation are mostly connected to the surface state of N-and metal ions dopant species in TiO_2 lattice, and to the peculiarities of the doping process (Ihnatiuk et al. 2017; Linnik et al. 2020). TiO_2 modified with different noble metals was intensively studied in the photocatalytic processes to clarify the effect of noble nanoparticle in photoinduced charge separation (Ahmed et al. 2014; Choi et al. 2010; Linnik et al. 2013; Ono et al. 2010). The photocatalyst immobilization in the form of a thin film breaks through the disadvantages of the powder form of photocatalyst: (1) the phases separation, (2) the difficulties to apply them to continuous flow systems, and (3) the tendency of the photocatalyst particles to be aggregated (Obalova et al. 2013).

It is believed that the high surface area of support materials is desired to provide dispersing of the metals, less aggregation and more available reactive sites which induce the electrocatalytic reaction (García et al. 2007). The activity of the composites based on the different ratio of metals (Pt/Ru, Pt/Ir, Pt/Ru/Ir, Ir/Ru) loaded on anatase or rutile toward the oxygen evolution reaction was significantly enhanced compared to unsupported metals NPs assuming the contribution of the supports in the formation of small and well-dispersed metal NPs on their surfaces (no essential effect of titania crystalline forms on electrocatalytic activity was observed) (Fuentes et al. 2011).

Recently, we have reported (Ihnatiuk et al. 2020) the effect of synthesis conditions on the surface Pt oxidation states formed in TiO_2 lattice that, in turn, change the optical, photocatalytic and morphological properties of the films. It was found that Pt^0 NPs (nanoparticles) are formed in the structure of the films as a result of the redox reaction occurring during sol ripening and calcination of the films at certain conditions. The incorporation of Pt ions in TiO_2 (Pt^{n+}–O–Ti) and Pt–O–Pt bonds formation fixed for some cases were proven by XPS data. It was shown that the enhanced photocatalytic activity was caused by the presence of Pt ions rather than Pt^0 NPs. Herein, the results of photoelectrochemical, photocatalytic and electrocatalytic investigations are reported. The photoelectrochemical characteristics, as namely the potentials of the conduction (CB) and valence (VB) bands, the bandgap energy as well as the quantum yield efficiency, and photocatalytic activity in N_2O decomposition recognized as relatively stable compound under ambient conditions causing the greenhouse effect and destructing of the ozone layer (Kočí et al. 2012, 2017) are analyzed to clarify the photocatalytic behavior of the samples. Catalytic properties of titania modified by Pt and N in an important electrocatalytic reduction of dissolved oxygen (OER) and hydrogen evolution (HER) reactions and their structural and surface peculiarities are also reported.

Materials and methods

The synthesis procedures of the films and electrodes have been performed as described in detail in Ihnatiuk et al. (2020). The samples used in photocatalytic experiments and photoelectrochemical investigations have been coated on glass slides and Ti sheets, respectively. Briefly, two different procedures have been used to synthesize titania films doped with 1 mol.% Pt(II) acetylacetonate and co-doped with 1 mol.% Pt(II) acetylacetonate and 5 mol.% urea. The samples marked as method 1 were synthesized using three-block copolymers of polyethyleneoxide and polypropyleneoxide $(PEO)_{20}(PPO)_{70}(PEO)_{20}$ (Pluronic 123) and acetylacetone to obtain the porous surface. The films of the second procedure (method 2) were a simple and fast performed way of mixing iso-propanol, $Pt(acac)_2$ dissolved in acetone and ethanol solution of urea (in the case of nitrogen-doped films). The three-layered films have been obtained by dip-coating procedure at a withdrawal rate of 1.5 mm/s. The films were calcinated at 450 °C for 20 min at the heating rate of 7 °C/min in the presence of air. The samples coded as $Pt(N)–TiO_{2\_M1(M2)\_UV}$ were additionally UV treated before calcination (see details in (Ihnatiuk et al. 2020).

The photoelectrochemical measurements have been performed using a quartz electrochemical cell, a high-pressure xenon lamp, a monochromator with a spectral resolution of 1 nm, three-electrode setup and 1 mol/L KCl electrolyte solution have been employed for the photoelectrochemical measurements (Fig. 1). Platinum and Ag/AgCl electrodes have been used as auxiliary and reference ones, respectively. The flat band potential (E_{fb}) has been determined by the photoelectrochemical measurements and estimated from photocurrent I_{ph} changes measured at the maximum plotted against applied potential by straight-line extrapolation of these dependencies to the abscissa.

Photocatalytic decomposition of N_2O induced by different types of light was carried out with and without the photocatalyst (i.e. photocatalysis and photolysis, respectively). Measurements were done in a stainless steel photoreactor with a volume of 180 mL (Fig. 2). The microscope slide covered by the film was placed in the photoreactor below the quartz glass window. to remove air from the reaction mixture, the reactor was purged by N_2O (1030 ppm of N_2O in He) for 10 min. Then the reactor was sealed and the gas probe was withdrawn to measure the N_2O content before irradiation. The photocatalytic reaction was started by switching on the 8 W Hg lamp ($\lambda_{max} = 254$ nm) or the 1400 mW LED with a collimative lens ($\lambda_{max} = 405$ nm) placed on the quartz glass window of the photoreactor. The gas probes were periodically taken and immediately analyzed on a Gas Chromatograph (Tracera GC/BID, Shimadzu) with a barrier discharge ionization detector equipped with a micropacked column. The reproducibility of photocatalytic experiments was verified by two repeated tests that were within the experimental errors.

The electrocatalytic activity of the obtained electrodes in oxygen and hydrogen ions reduction was studied under potentiodynamic conditions using a PC-based electrochemical setup with the following characteristics: measured currents from 2×10^{-9} A to 10^{-1} A, potential scan rate in the range of 0.01–50 mVs^{-1}, working electrode potential range was set from − 4 to + 4 V. The measurements were performed in 0.9% NaCl solution at potentials 0/− 1.5 V vs. Ag/AgCl electrode.

To study the effect of additional irradiation, a second set of the obtained films were immersed in a solution of 0.9 wt% NaCl in DIW with the following illumination by an Oriel Xe–Hg 75 W arc lamp at 2 suns of intensity for 2 h. Light exposure was done for each film in a freshly prepared solution.

TEM and EDS images were obtained with a JEOL JEM-2800 (JEOL Ltd., Tokyo, Japan) at 200 kV of accelerating voltage and a large angle high-speed energy dispersive spectrometer (EDS) with an energy resolution of 133.0 eV. The mean particle size of Pt^0 was obtained from HR-TEM images by taking average by measured 30–50 particles.

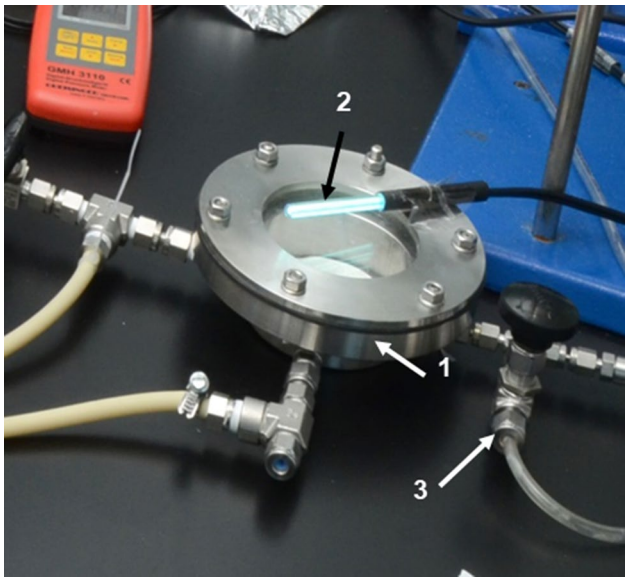

Fig. 2 An image of photocatalytic setup for N_2O decomposition: a photoreactor (1), light source (2) and gas flow (3)

Results and discussion

Photoelectrochemical characteristics of the films used as the working electrodes in a photoelectrochemical cell allow determining the energetic parameters of the semiconductive systems and finding out the influence of synthesis conditions as well as the surface composition on their photocatalytic and electrocatalytic properties.

The indirect transition bandgap energy (E_g) and flat band potential (E_{fb}) values obtained from photoelectrochemical data for TiO_2 electrode corresponding to 3.17 eV and − 0.51 V (Fig. 3, Table 1), respectively, are in good agreement with the reported value for bulk titania (Beranek et al. 2007; Kisch et al. 2007). The optical bandgap energies reported in our investigation were 3.6–3.7 eV (Ihnatiuk et al. 2020) and coincided with the values reported in the literature for the thin films (Frindell et al. 2002; Ismail and Bahnemann 2010; Krishna et al. 1993). It suggests the

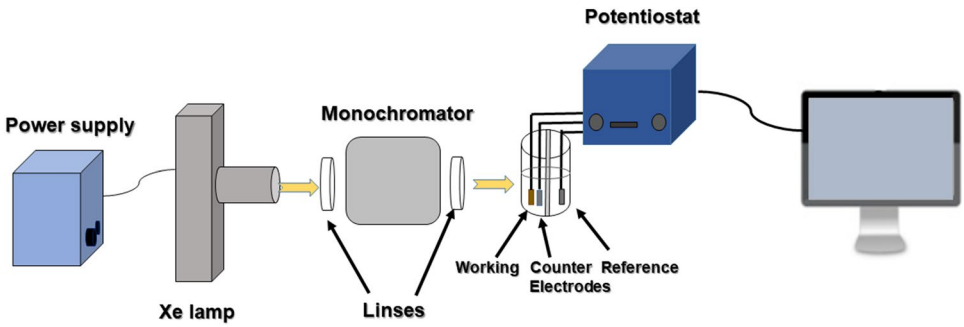

Fig. 1 A scheme of the photoelectrochemical setup

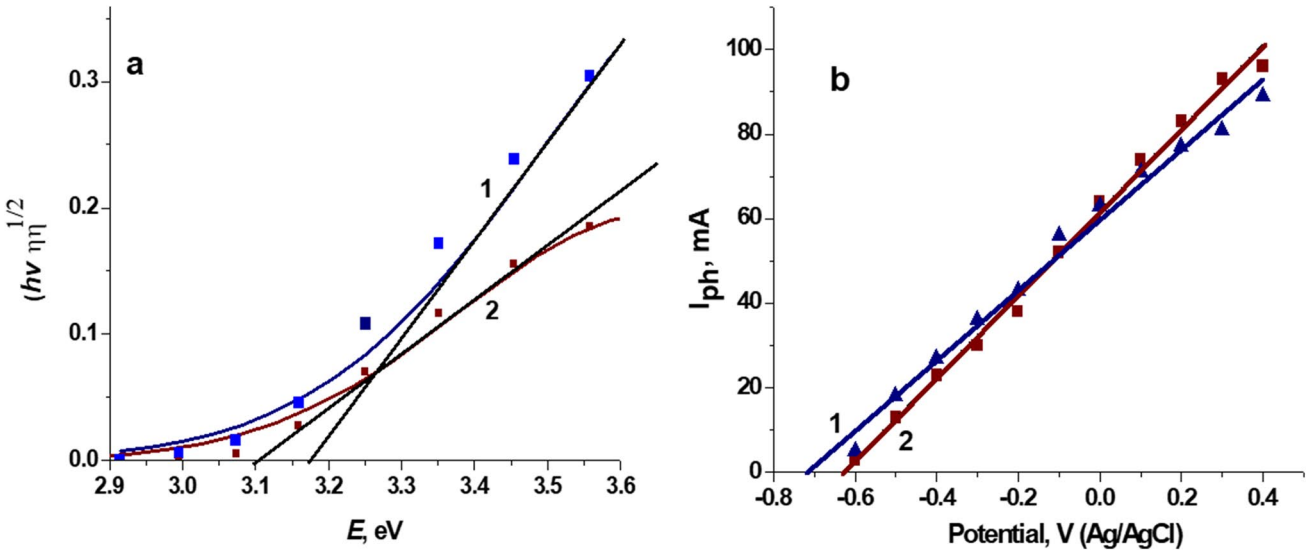

Fig. 3 $(h\nu\eta)^{1/2}$ as a function of E (**a**) and photocurrent *vs.* applied potentials (**b**) using TiO_2 (1) and N–TiO_2 (2) electrodes. Symbols and lines represent the experimental and fitted data, respectively

Table 1 Characteristics of the electrodes: the bandgap energy (E_g), the flat band potentials (E_{fb}), the valence band position (E_{VB}) vs. NHE and the deviation of the E_{fb} and E_{VB} values from the titania one ("+" and "−" signs express the anodic and cathodic shift, respectively)

Electrode	E_g, eV	E_{fb}, V	Δ_{fb}, V	E_{VB}, V	Δ_{VB}, V
TiO_2	3.17	− 0.51	0.00	+2.66	0.00
N–TiO_2	3.10	− 0.44	+0.07	+2.66	0.00
Method 1					
Pt–TiO_{2_M1}	3.13	− 0.42	+0.09	+2.71	+0.05
Pt,N–TiO_{2_M1}	3.06	− 0.41	+0.10	+2.65	− 0.01
Pt–$TiO_{2\_M1\_UV}$	3.06	− 0.40	+0.11	+2.66	0.00
Pt,N–$TiO_{2\_M1\_UV}$	3.03	− 0.38	+0.13	+2.65	− 0.01
Method 2					
Pt–TiO_{2_M2}	2.96	− 0.39	+0.12	+2.57	− 0.09
Pt,N–TiO_{2_M2}	2.98	− 0.41	+0.10	+2.57	− 0.09
Pt–$TiO_{2\_M2\_UV}$	2.92	− 0.41	+0.10	+2.51	− 0.15
Pt,N–$TiO_{2\_M2\_UV}$	2.92	− 0.44	+0.07	+2.48	− 0.18

crystallization of titania particle size below 3 nm that leads to a shift of the absorption band edge to the shorter wavelengths in the optical spectra (Kisch 2015). The decreased E_g value (3.10 eV) and a shift of E_{fb} potential for N–TiO_2 compared to TiO_2, shown in Fig. 1, can be explained by the crystallization of the mixture of anatase and brookite (Ihnatiuk et al. 2020) in the approximated composition of 23% and 77%, respectively. As the synthesis of pure crystalline brookite form (without anatase and rutile) is quite difficult, there are numerous uncertainties related to its bandgap as well as to the energy position of the conduction band (Di Paola et al. 2013; Ismail et al. 2010; Shibata et al. 2004). The bandgap energy (3.14 eV) and the flat band potential (− 0.03 V) of brookite situated between anatase and rutile ones analogous to calculated LUMO energies were reported by (Grätzel and Rotzinger 1985). It was shown that the difference of E_g and E_{fb} values of anatase and brookite were $\Delta E_g = 0.09$ eV and $\Delta E_{fb} = \sim 0.09/0.11$ V whereas brookite and rutile were $\Delta E_g = 0.12$ eV and $\Delta E_{fb} = 0.03$ V coinciding with the obtained data herein. It has to be noted that there is no visible effect of urea modification on the valence band position of N–TiO_2 film.

The E_g values determined at 3.03–3.13 eV for the Pt-containing electrodes obtained by method 1 are close to the values of non-Pt-doped films (Fig. 4, Table 1). Since the crystallization of the only anatase was detected for these films as shown by our investigation in (Ihnatiuk et al. 2020), the obtained E_g values have to be compared with TiO_2 one. Therefore, the decrease in these values is most probably connected to the presence of Pt species that are inhomogeneously distributed over the surface and bulk as shown by XPS and EDS data (Ihnatiuk et al. 2020).

The narrowing of bandgap to 2.98–2.92 eV of the method 2 electrodes consisted of anatase as well (Ihnatiuk et al. 2020) can be a result of higher atomic content of Pt that is homogeneously distributed over surface layer and bulk due to the low efficiency of Pt^0 formation (Table 2). The E_g values of 2.96–2.98 eV are observed for the samples contained Pt^{2+}–O–Ti bonds, while the most narrowing (2.92 eV) is noted for the samples with Pt^{2+}–O—Pt and/or Pt^{4+}–O–Ti fragments (Table 2).

Assuming that the flat band potential represents the lowest edge of the conduction band and taking into account the anatase crystallization in Pt-doped films, the shift to more

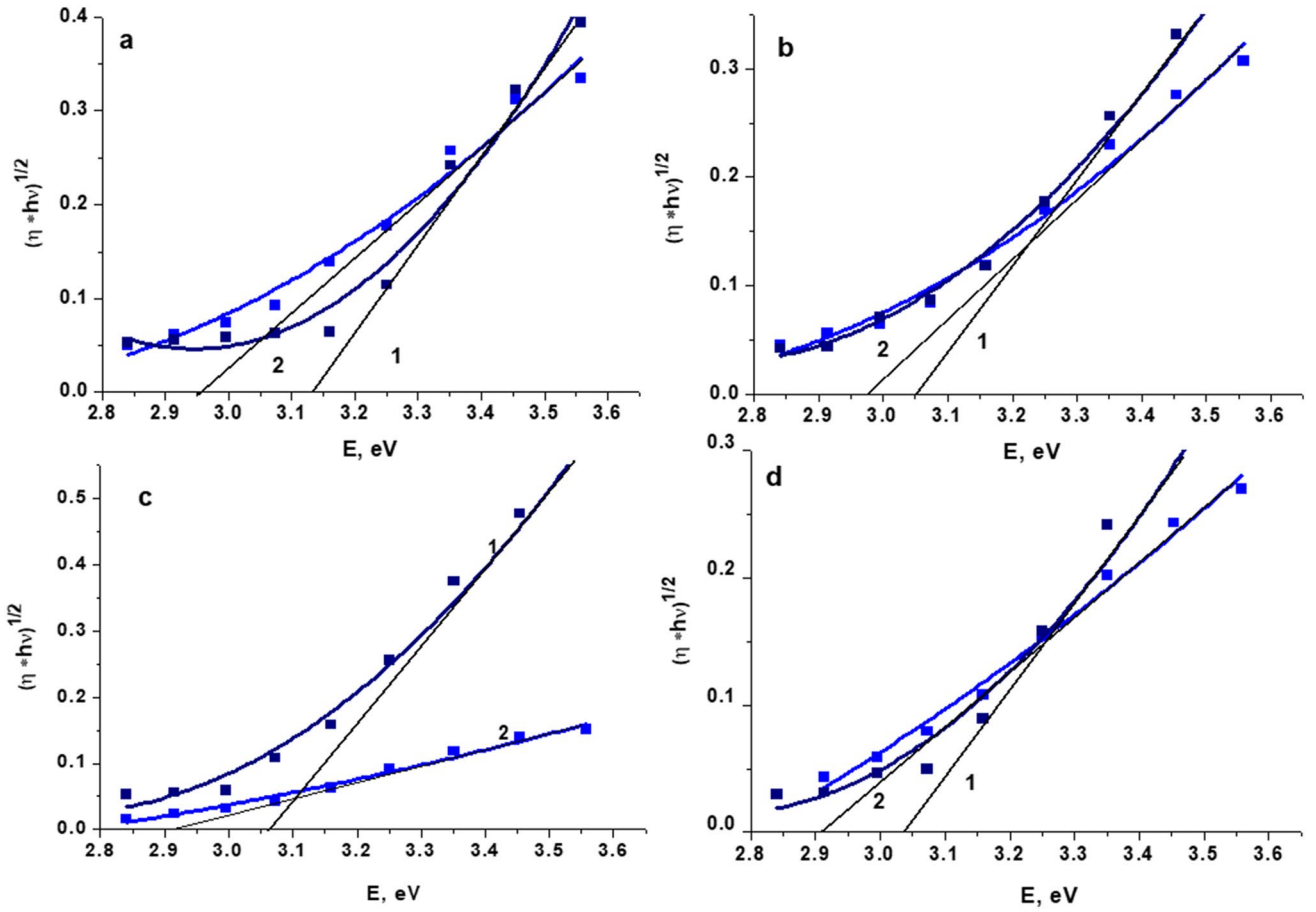

Fig. 4 Dependence of $(h\nu\eta)^{1/2}$ on the energy of incident light using the electrodes obtained by method 1 (curve 1) and method 2 (curve 2): Pt–$TiO_{2\_M1(M2)}$ (**a**), Pt,N–$TiO_{2\_M1(M2)}$ (**b**), Pt–$TiO_{2\_M1(M2)\_UV}$ (c) and Pt,N–$TiO_{2\_M1(M2)\_UV}$ (**d**). Squares and lines represent the experimental and fitted data, respectively

Table 2 Atomic content (AC) and relative atomic content (RAC) of Pt species on the surface of the films obtained from XPS data

Film	Pt	Pt^0	Pt^{2+}–O–Ti	Pt	Pt^0	Pt^{2+}–O–Ti	Pt^{2+}–O–Pt	Pt^{4+}–O–Ti
	AC, %	RAC·10^{-2}		AC, %	RAC·10^{-2}			
	Method 1			Method 2				
Pt–$TiO_{2\_M1(M2)}$	0.13	1.5	11.5	0.40	–	40.0		–
Pt,N–$TiO_{2\_M1(M2)}$	0.16	12.3	3.7	0.35	6.8	10.2	15.9	2.0
Pt–$TiO_{2\_M1(M2)\_UV}$	0.30	16.7	13.4	0.45	–	–	37.5	7.3
Pt,N–$TiO_{2\_M1(M2)\_UV}$	0.11	4.4	6.6	0.20	3.0	–	11.0	6.0

positive potentials (Fig. 5, Table 1) compared to TiO_2 can be explained by Pt incorporation in TiO_2 lattice as shown by XPS investigation (Pt^{n+}–O–Ti bonds) (Ihnatiuk et al. 2020). It seems that the E_{fb} position is correlated with the relative atomic content (RAC) of Pt^{n+}–O–Ti fragments in the case of electrodes obtained by method 2: the most positive value is obtained for Pt–TiO_{2_M2} electrode containing the highest RAC of Pt^{2+}–O–Ti fragments whereas the most negative value belongs Pt,N–$TiO_{2\_M2\_UV}$ sample where the surface contains the lowest RAC of Pt^{4+}–O–Ti fragments (Tables 1, 2).

The position of the valence band edge (E_{VB}) is estimated from E_g and E_{fb} assuming $E_{fb} \sim E_{CB}$. The energetic positions of E_{VB} of method 1 electrodes coincides with TiO_2 excepting Pt–TiO_{2M1} electrode where E_{VB} is shifted to more positive values by 5 mV. The significant cathodic shift (9–18 mV) of E_{VB} for method 2 electrodes is observed. As the valence band presents the energetic characteristics of anions in the

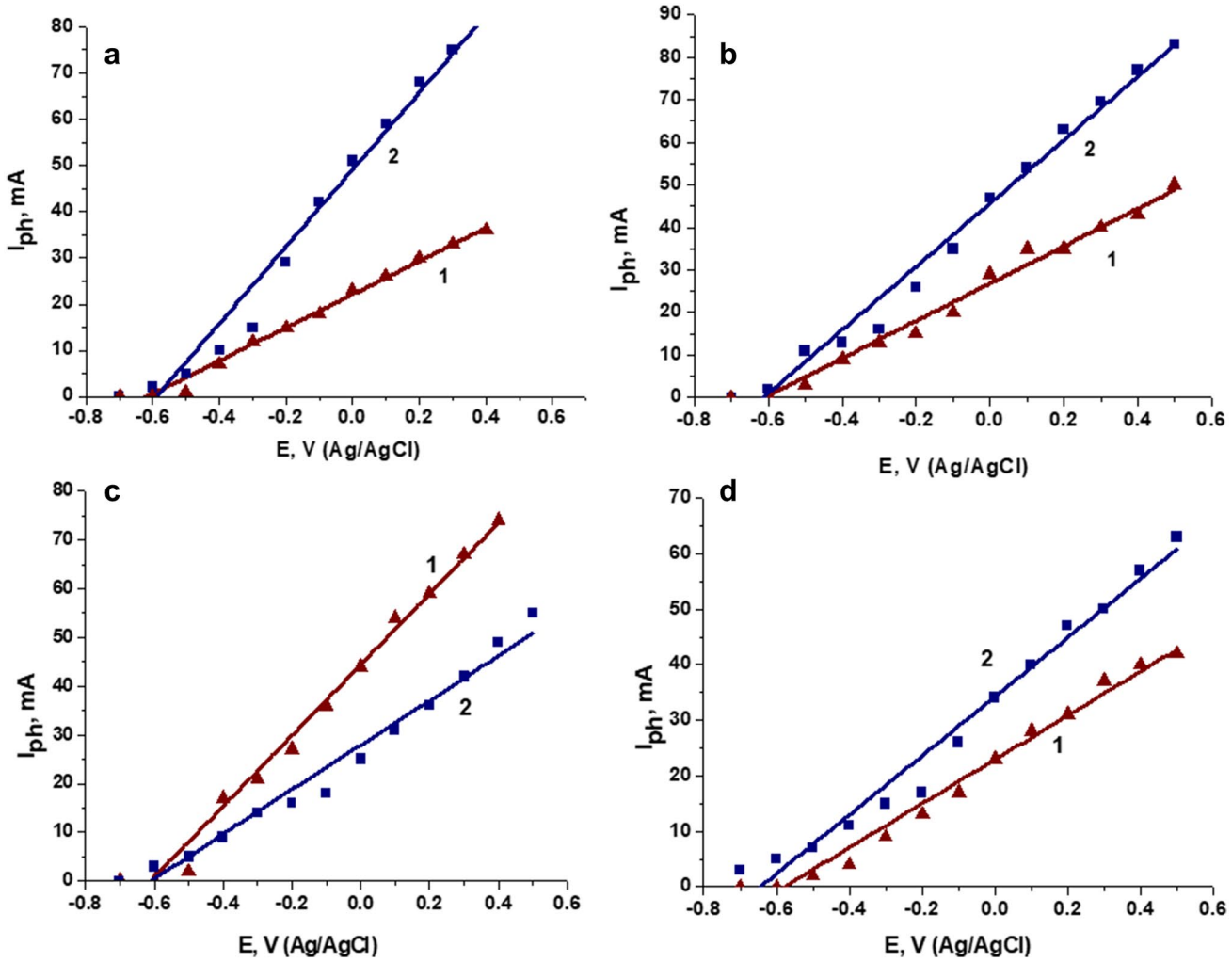

Fig. 5 Photocurrent as a function of applied potentials obtained for Pt–$TiO_{2\_M1(M2)}$ (**a**), Pt,N–$TiO_{2\_M1(M2)}$ (**b**), Pt–$TiO_{2\_M1(M2)\_UV}$ (**c**) and Pt,N–$TiO_{2\_M1(M2)\_UV}$ (**d**) electrodes of method 1 (1) and method 2 (2)

electronic structure of titania, the formation of the defects as a result of Pt^{n+} incorporation can be considered (Choi et al. 2010; Choudhury et al. 2013; Serpone 2006). It is known that ionic radii (r) of Pt^{2+} and Pt^{4+} are 0.94 Å and 0.765 Å, respectively, assuming their location in TiO_2 lattice ($r = 0.745$ Å) in the different positions: Pt^{2+} in the interstitial one and Pt^{4+} in the form of a substitutional atom (Choi et al. 2010). The more positive values of VB were reported (Smirnova et al. 2006) for mixed (0–50%)ZrO_2/TiO_2 systems where the crystallization of only anatase was detected by XRD while the XPS results clearly point on the formation of Zr–O–Ti bonds (Gnatyuk et al. 2010). The interstitial position of Zr^{4+} ions ($r = 0.86$ Å) can be predicted similar to Pt^{2+} ones due to much higher ionic radius of Zr. Since the RAC of inhomogeneously distributed Pt^{2+}–O–Ti fragments of method 1 films is low (Tab. 2), the obvious change in E_{VB} is not noted contrary to the films of method 2. Additionally, the incorporation of Pt^{4+} in TiO_2 can be a reason for the significant deviation in E_{VB} for Pt–$TiO_{2\_UV\_M2}$ and Pt,N–$TiO_{2\_UV\_M2}$ films due to the formation of oxygen defects in semiconductive lattice. No direct evidence of N effect on the position of E_{VB} is observed for N and Pt co-doped materials.

Quantum yield (QY) of photocurrent fixed at the high energy light (4.72 eV) using the electrodes obtained by method 1 showed a similar behavior to TiO_2 that can be a result of low Pt content at the film surfaces (Table 3 and Fig. 6). However, its values are decreased by 4–10 times for method 2 electrodes compared to method 1 suggesting the faster recombination of photogenerated charges due to the presence of homogeneously distributed Pt^{2+} ions. When the energy of incident light is lowered to 3.16 eV and 3.07 eV, the quantum yield becomes more correlated with Pt^0 atomic content for method 1 films (Fig. 7a) and the relative atomic content of Pt^{n+}–O–Ti fragments in the case of method 2 (Fig. 7b): the higher the atomic content of Pt^0 and relative

Table 3 Quantum yield obtained at the presence of the electrodes at different energies of the incident light

Electrode	QY × 10^{-3} 262 nm 4.72 eV	QY × 10^{-3} 392 nm 3.16 eV	QY × 10^{-3} 403 nm 3.07 eV	QY × 10^{-3} 425 nm 2.91 eV
TiO_2	28.2	5.2	1.7	0.0
N–TiO_2	5.4	3.3	1.2	0.5
Method 1				
Pt–TiO_{2_M1}	29.2	1.3	1.3	1.1
Pt,N–TiO_{2_M1}	17.5	4.4	2.5	0.7
Pt–$TiO_{2\_M1\_UV}$	36.5	7.9	3.8	1.1
Pt,N–$TiO_{2\_M1\_UV}$	23.4	2.5	0.8	0.3
Method 2				
Pt–TiO_{2_M2}	2.4	6.1	2.8	1.3
Pt,N–TiO_{2_M2}	4.9	4.5	2.3	1.1
Pt–$TiO_{2\_M2\_UV}$	7.3	3.5	1.7	0.6
Pt,N–$TiO_{2\_M2\_UV}$	4.9	3.7	2.1	0.7

atomic content of Pt^{2+}–O–Ti are, the higher its values are observed for method 1 and method 2 electrodes, respectively.

At energy equals to 2.91 eV, titania does not absorb the quantum of light whereas N–TiO_2 exhibited quite a low absorption activity (Table 3) that, surely, is connected with the modification by urea, namely the presence of interstitial N in the form of –C–N=C–fragments (XPS is available herein (Supplementary materials in Ihnatiuk et al. 2020). The electrodes synthesized by method 1 exhibited the lower quantum yield for N-modified Pt–TiO_{2_M1} that can be caused by urea modification. Quantum yield at 3.16, 3.07 and 2.91 eV of method 2 electrodes is decreased for the Pt–$TiO_{2\_M2\_UV}$ and Pt,N–$TiO_{2\_M2\_UV}$ containing the O–Pt^{2+}–O and Pt^{4+}–O–Ti fragments.

To understand the impact of co-doping by Pt and N on the photocatalytic properties of the materials, the decomposition of N_2O was studied under UV (254 nm) and visible (405 nm) irradiation (Fig. 8). Conversion of N_2O in the presence of the films was more efficient regardless of the energy of irradiation compared to the photolysis. In the case of UV irradiation, the highest conversion of N_2O was registered in presence of Pt,N–TiO_{2_M1} and TiO_2. It is obvious that the doping of titania does not improve the films' photoactivity under irradiation at 254 nm (Fig. 6a) as the efficiency of N_2O conversion over the doped films was similar or lower compared to TiO_2 one. However, the highest conversion degree of N_2O was observed over Pt,N–$TiO_{2\_M1(M2)}$ films independently on the synthesis procedure under visible irradiation (Fig. 8b). It is clear that the co-doping by metal and non-metal elements plays a key role in photocatalytic reaction. Metal and non-metal co-doping of TiO_2 results in the synergistic effect of inhibition of recombination process and the narrowing of the band gap energy (Liu et al. 2016; Meng et al. 2012). Taking into account the presence of substitutional N, N in the form of –C–N=C–fragments and different Pt species as shown by XPS data (Table 2), an electron and a hole can be trapped resulting in the decrease of recombination processes. Consequently, the generated electron and holes can be used for redox reaction and subsequently increased efficiency in N_2O photocatalytic decomposition (Fig. 8b).

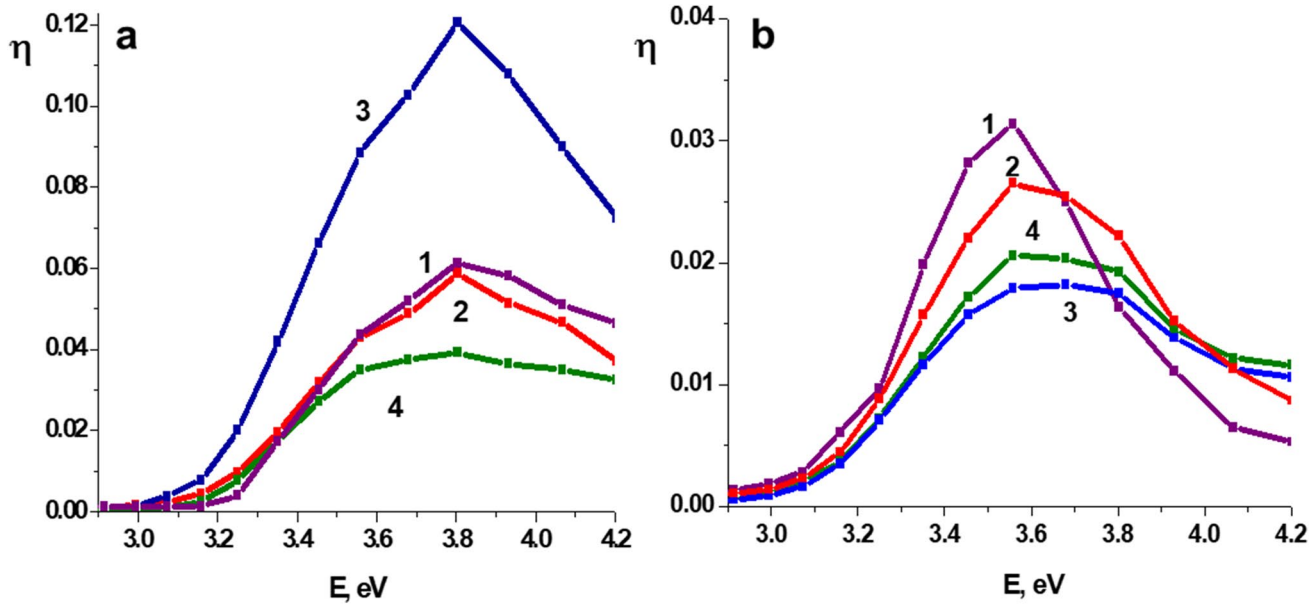

Fig. 6 Quantum yield efficiency of method 1 (**a**) and method 2 (**b**) electrodes: Pt–$TiO_{2\_M1(M2)}$ (1), Pt,N–$TiO_{2\_M1(M2)}$ (2), Pt–$TiO_{2\_M1(M2)\_UV}$ (3), Pt,N–$TiO_{2\_M1(M2)\_UV}$ (4)

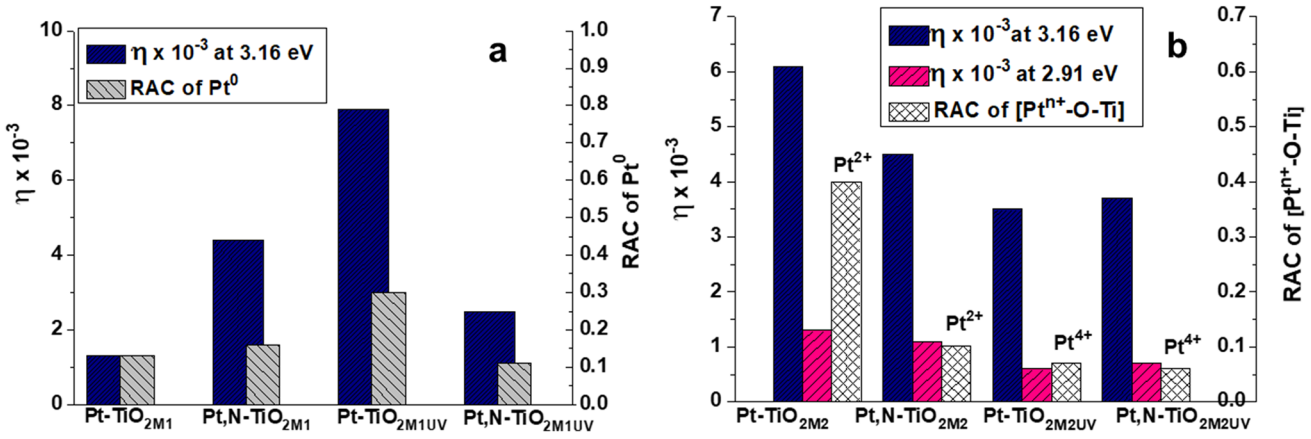

Fig. 7 Correlation between the quantum yield and Pt species on the film surfaces for the electrodes synthesized by method 1 (**a**) and method 2 (**b**)

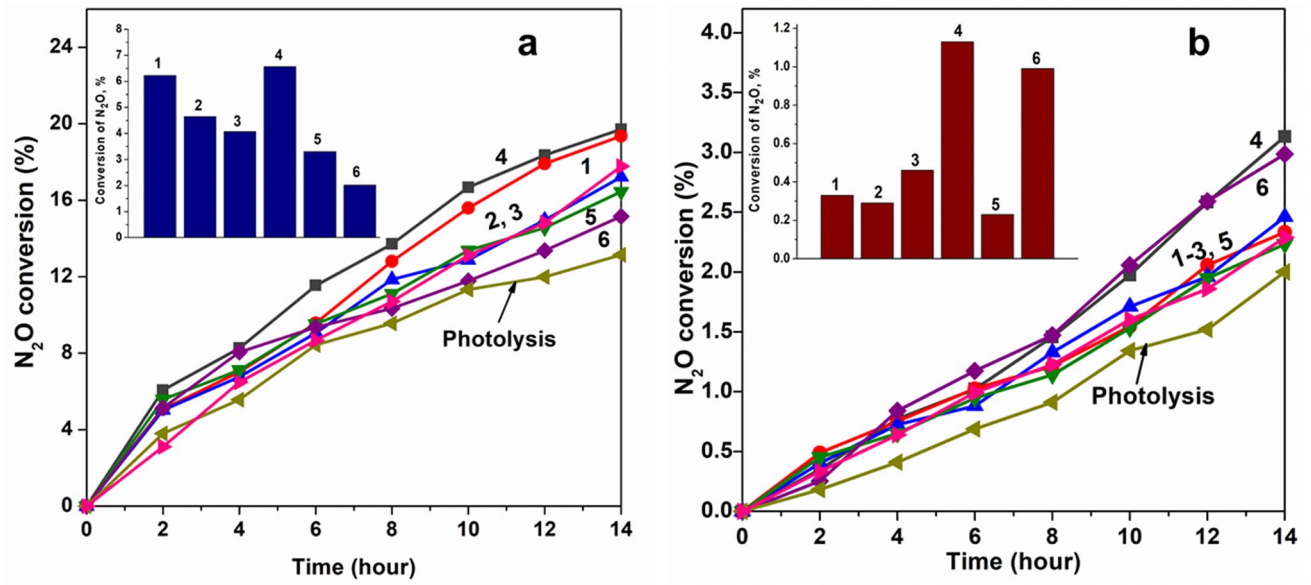

Fig. 8 Photocatalytic decomposition of N_2O over TiO_2 (1), N–TiO_2 (2), Pt–TiO_{2_M1} (3), Pt,N–TiO_{2_M1} (4), Pt–TiO_{2_M2} (5) and Pt,N–TiO_{2_M2} (6) films under UV (**a**) and visible (**b**) irradiation. Insert represents the difference between N_2O conversion over a film and photolysis for 14 h irradiation

The band gap energy of Pt,N–TiO_{2_M1} and Pt,N–TiO_{2_M2} is lowered (3.06 and 2.98 eV, respectively) in comparison with pure TiO_2 (3.17 eV) (Table 1) leading to absorption of the lower energy light (Fig. 6b). The highest activity in N_2O decomposition under both UV and visible light is noted for Pt,N–TiO_{2_M1} film whereas Pt,N–TiO_{2_M2} exhibits the activity only under visible irradiation. The inactivity of the last film under UV irradiation can be caused by near two times lower RAC content of Pt^0 compared to the former one (Table 2) taking into account that the certain content of Pt^0 loaded on titania can act as a photogenerated electron scavenger preventing the recombination of photoformed charges (Ahmed et al. 2014).

It is known that Pt is the effective catalyst for HER but the growing demands of this reaction require the creation of highly active and less expensive materials. One of the possible ways to decrease the expense of the reaction is to consider the support metallic NPs of platinum group metals (Danilovic et al. 2012; Bernsmeier et al. 2019; Subbaraman et al. 2011). The hydrogen adsorption free energy is responsible for the electrocatalytic activity of a catalyst in HER as suggested in the "volcano" plot reported in Parson

(1957). Two types of metal hydride bonds on the surface are believed to be formed: a strong adsorption of the H and a weak one to promote the H_2 formation (Eftekhari 2017). The efficiency of HER depended on the particle size and surface morphology of Pt electrocatalysts as reported in Li et al. (2015). Therefore, Pt-doped films have been tested for HER to elucidate their activity in this process and the possible active sites for H^+ adsorption (Table 4 and Fig. 9).

Electrocatalytic HER at potentials from − 0.8 to − 1.3 V is fixed over all Pt-doped TiO_2 electrodes while Pt-free ones are inactive. The most active electrodes for this reaction are Pt/TiO_{2_M2} and Pt,N–TiO_{2_M2} whereas the electrodes obtained by method 1 exhibited much lower activity with the most inactive one Pt,N–TiO_{2_M1}. Analyzing the surface oxidation states and the formed bonds of Pt species (Table 2), it is suggested that the Pt^{2+}–O–Ti fragments are responsible for activity in HER at the reported conditions. It is recently shown by experimental investigation and DFT calculations (Yu et al 2020) that the Pt–O bonds in polyoxometalates can be responsible for electrocatalytic activity in the process of hydrogen evolution reaction. It is stressed that the Pt–O site accelerates the coupling of electron and proton resulting in a rapid release of H_2. Thus, knowing that the Pt–TiO_{2M2} film exhibiting the highest activity contains the highest relative atomic content of Pt^{2+}–O–Ti fragments, whereas the Pt,N–TiO_{2_M1} film showing the poorest response has the lowest content of these bonds, the activity in HER is signed to the presence of Pt^{2+}–O–Ti bonds.

The Pt- and Pt,N-doped titania films were also tested in EOR at potentials from − 0.5 to − 0.8 V. The more positive value of half-wave potentials obtained using these films point to a slightly higher electrocatalytic activity compared to TiO_2 and N–TiO_2 ones (Table 4 1st cycle). However, an additional UV exposure of the electrodes used in this reaction (Table 4 2nd cycle) led to significant improvement of electrocatalytic properties of some films that can be seen

Table 4 Half-wave potential $E_{1/2}$ of O_2 evolution and electrode potential of H_2 evolution

Film	E (H_2) at − 10 mA/cm^2, V		$E_{1/2}$(O_2), V			
	Method 1	Method 2	Method 1		Method 2	
			1st cycle	2nd cycle	1st cycle	2nd cycle
TiO_2	Inactive		− 0.60			
N–TiO_2	Inactive		− 0.58			
Pt–$TiO_{2\_M1(M2)}$	− 1.44	− 1.36	− 0.55	− 0.55	− 0.55	− 0.50
Pt,N–$TiO_{2\_M1(M2)}$	− 1.61	− 1.40	− 0.55	− 0.55	− 0.55	− 0.53
Pt–$TiO_{2\_M1(M2)\_UV}$	− 1.43	− 1.44	− 0.55	− 0.52	− 0.55	− 0.55
Pt,N–$TiO_{2\_M1(M2)\_UV}$	− 1.42	− 1.45	− 0.55	− 0.49	–	− 0.54

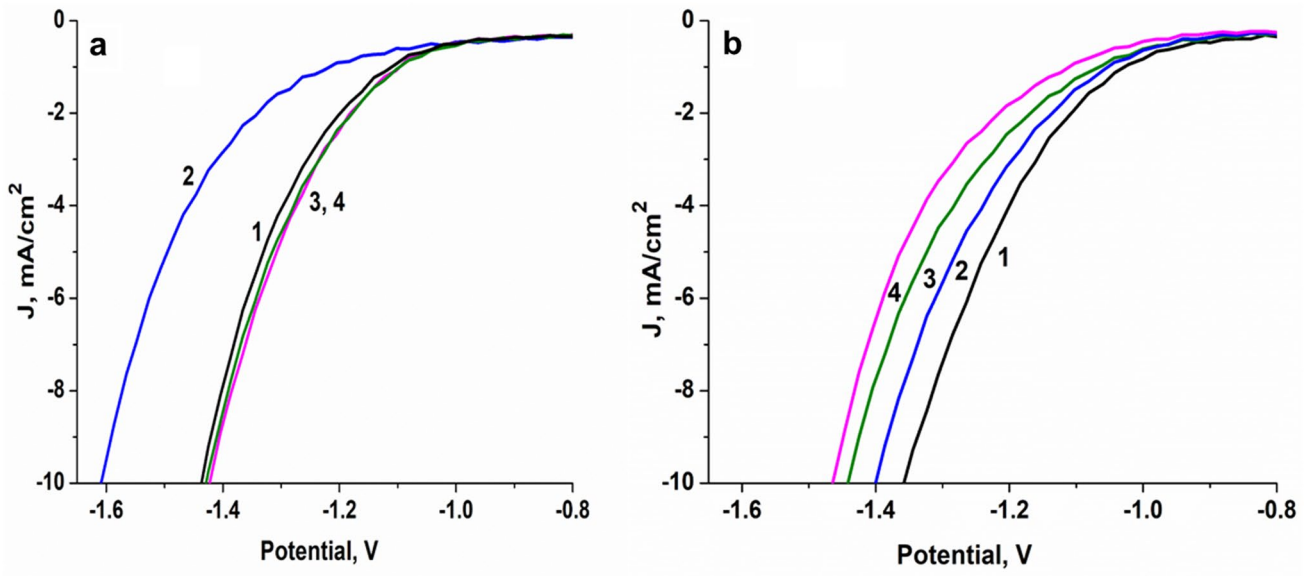

Fig. 9 Polarization curves of the electrodes vs. Ag/AgCl electrode obtained by method 1 (**a**) and method 2 (**b**): Pt–$TiO_{2\_M1(M2)}$ (1), Pt,N–$TiO_{2\_M1(M2)}$ (2), Pt–$TiO_{2\_M1(M2)\_UV}$ (3) and Pt,N–$TiO_{2\_M1(M2)\_UV}$ (4)

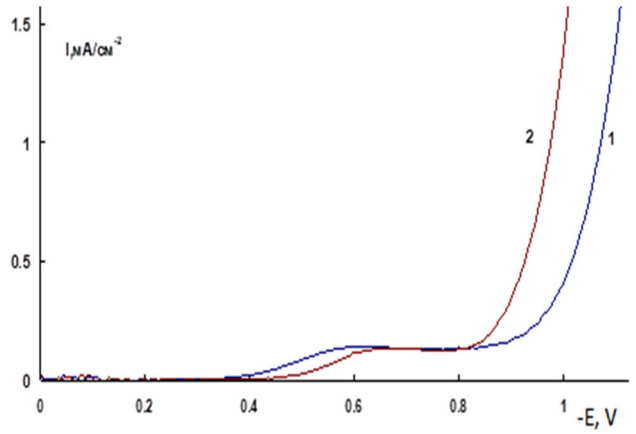

Fig. 10 Current density vs. applied potentials for Pt,N–$TiO_{2\_M1\_UV}$ electrode (1–2nd cycle and 2–1st cycle)

from the shift of the potential curves (Fig. 10). The highest activity among the samples is observed for Pt–$TiO_{2\_M1\_UV}$ and Pt,N–TiO_{2_M2}. The Pt,N–$TiO_{2\_M2\_UV}$ electrode that was inactive during the first cycle showed some activity after the second exposure.

The improvement of electrocatalytic properties after exposure of UV light in OER could be suggested by the enrichment of the surface by Pt^0 due to the reduction of Pt^{2+} ions to Pt^0 or to the change of hydrophilic properties of the surface (Meng et al. 2017). We have shown in (Ihnatiuk et al. 2020) that Pt^0 NPs were formed in the structures due to the presence of organic compounds in the precursor sols: Pluronic123 and acetylacetone in the case of method 1 or urea in the case of films synthesized by method 2. To check out the effect of UV irradiation on the Pt^0 formation and its distribution, TEM and EDS investigations were performed (Fig. 11, Table 5) for the films subjected to additional UV irradiation in 0.9 wt% NaCl solution. It is obvious

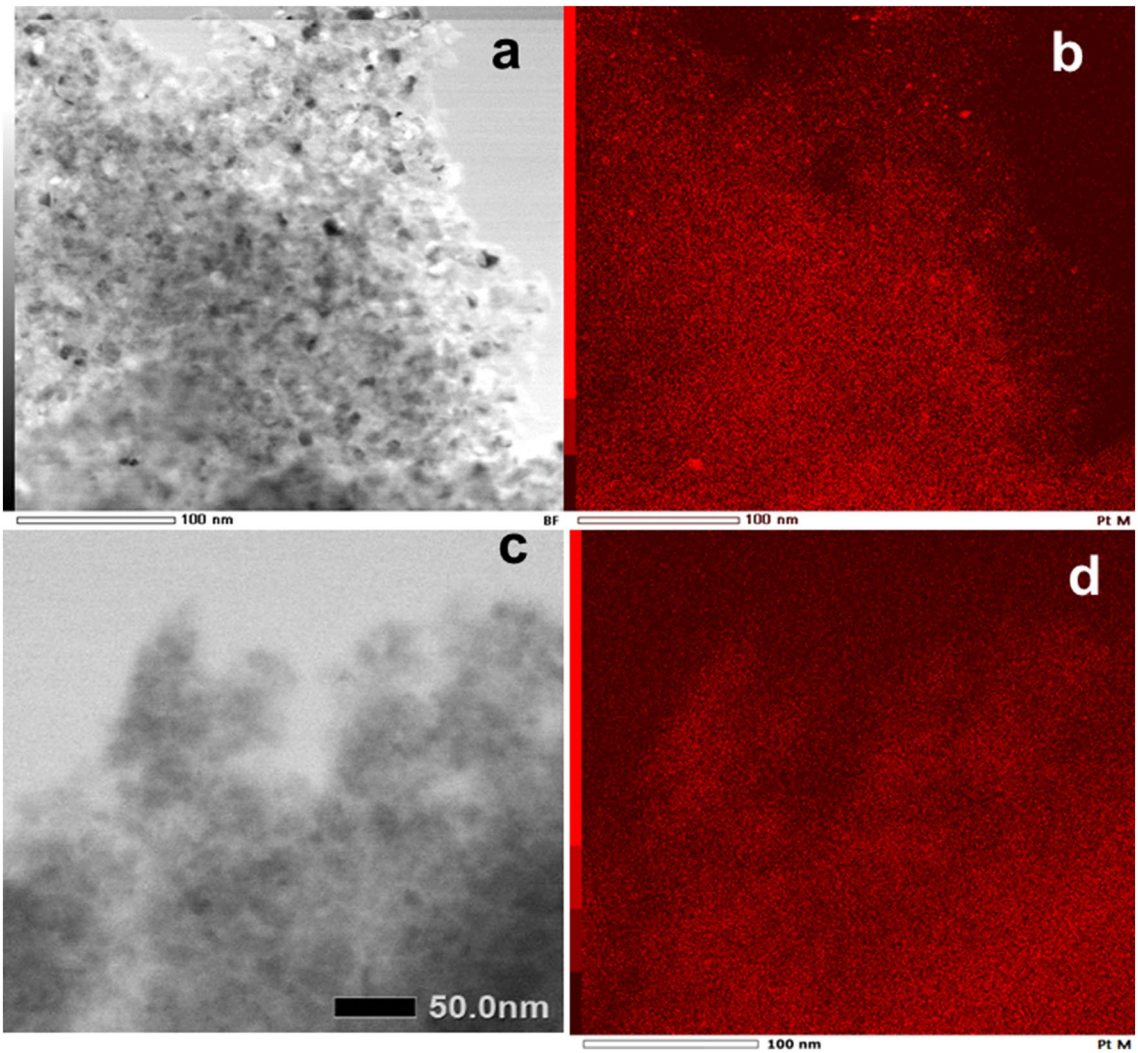

Fig. 11 TEM images (**a**, **c**) and EDS mappings (**b**, **d**) for Pt element of Pt,N–TiO_{2_M1} (**a**, **b**) and Pt–TiO_{2_M2} (**c**, **d**) films

Table 5 The atomic content and ratio of the elements before and after UV exposure obtained from EDS data for Pt,N–TiO_{2_M1} and Pt–TiO_{2_M2} films

UV exposure	Ti	O	Pt	Ti:O:Pt
	Atomic content, %			Atomic ratio
Pt,N–TiO_{2_M1}				
No	33.99	65.66	0.36	1.000:1.932:0.011
After	35.81	64.89	0.58	1.000:1.812:0.016
Pt–TiO_{2_M2}				
No	31.98	67.68	0.34	1.000:2.116:0.011
After	48.02	51.34	0.64	1.000:1.069:0.013

that Pt,N–TiO_{2M1} sample contains Pt^0 NPs with an average size of 7.3 ± 2.8 nm that is almost two times higher than before irradiation (3.3 ± 0.4 nm (Ihnatiuk et al. 2020)). It must be noted that no detectable Pt^0 NPs are observed for Pt–TiO_{2M2} that can be caused by Pt^{2+} incorporation in the form of Pt^{2+}–O–Ti bonds preventing Pt^0 aggregation. The ratio of Pt to Ti is almost unchanged for the last film contrary to the former case where Pt content is significantly increased after UV irradiation.

Considering the effect of UV light on Pt,N–TiO_{2_M1} films, the following mechanism is proposed (Fig. 12a). As known, the reduction of Pt^{2+} ions to Pt^0 follows through a two electrons process that can be fulfilled due to the previously formed Pt^0 NPs deposited on the surface of the titania particle. A quantum of UV light absorbed by TiO_2 generates an electron–hole pair. An electron can be effectively trapped by Pt^0 NPs (Fig. 12a, pathway 1) while a hole participates in the oxidation reaction of a surface hydroxyl group. A new portion of light drives out to the next electron into the Pt^{2+} sublevel or the conduction band of TiO_2 leading to Pt^{1+} formation (Fig. 12a, pathway 2). A transfer of trapped by Pt^0 NP electron to Pt^{1+} species (Fig. 12a, pathway 3) can occur due to an accumulation of Pt species, as shown by EDS, causing a favorable interfacial electron transfer. The deposition of UV-formed Pt^0 onto Pt^0 NPs (Fig. 12a, pathway 4) can be confirmed by Pt^0 NPs size growth and higher nonhomogeneity.

Since no detectable Pt^0 NPs in Pt–TiO_{2_M2} sample are observed after UV exposure (Fig. 11c, d) as well as taking into account the homogeneous distribution of Pt^{2+} in TiO_2 lattice, it is supposed that the reduction Pt^{2+} ions to Pt^0 does not occur under UV irradiation. In the absence of Pt^0 NPs, as seen from Fig. 12b, the photogenerated electrons can be subjected to the trapping by Pt^{2+} with the following interaction with O_2 molecule (Fig. 12b, pathways 1 and 3) or recombining with a hole (Fig. 12b, pathway 2) at the present conditions.

Therefore, the improved electrocatalytic activity in OER is most probably connected to the increased hydrophilicity of TiO_2 surface after UV irradiation leading to the improved adsorption of hydroxyls (dissociated water) (Wang et al. 1998; Wei et al. 2020) as well as desorption of O_2 molecules.

Conclusions

It is shown that the synthesis conditions of Pt- and Pt,N-doped titania films influence the film composition and oxidation states of the Pt species that, in turn, change the electronic structure of materials, photocatalytic and electrocatalytic properties. The bandgap values of the semiconductive materials significantly decreased in the case of homogeneously distributed Pt species of certain content. The flat band potentials are correlated with the relative atomic content of Pt^{n+}–O–Ti fragments. The valence band edge is shifted to more negative values that can be a result of Pt^{4+} ions incorporation leading to the formation of oxygen defects in the lattice of the semiconductor.

It is found that the quantum yield at the incident light energy of 3.16 eV and 3.07 eV correlates with Pt^0 atomic content and the relative atomic content of Pt^{n+}–O–Ti fragments. The decrease in quantum yield values can be associated with the formation of N-and Pt^{n+}-containing fragments acting as an electron and a hole trap.

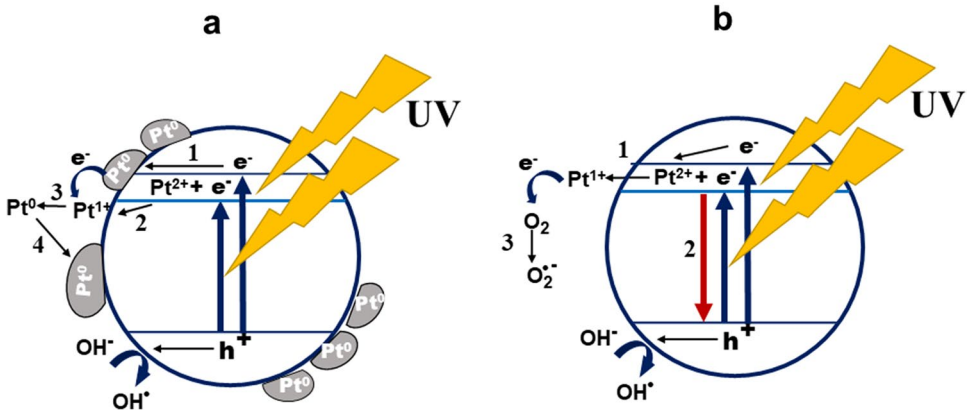

Fig. 12 The proposed mechanisms of UV action for the films containing (**a**) and without (**b**) Pt^0 NPs

The highest activity for N_2O photocatalytic decomposition is observed for Pt,N–TiO_2 films. The key role is assigned to co-doping of TiO_2 by metal (Pt) and non-metal (N) elements. Metal–non-metal–TiO_2 modified films result in synergistic effect including (1) inhibition of recombination of electrons and holes and (2) narrowing of the band gap.

The investigation of electrocatalytic properties indicates that the Pt–TiO_{2_M2} sample containing only Pt^{2+}–O–Ti bonds is active in the HER process. The additional UV exposure of the electrodes led to significant improvement of OER for Pt–TiO_{2_M2} and Pt,N–$TiO_{2\_M1\_UV}$. No detectable by EDS mapping Pt^0 NPs are noted for the film consisting only of incorporated Pt^{2+} ions, therefore, the improved activity in OER can be connected with higher hydrophilicity of the surface. The mechanisms of the Pt^{2+} photoreduction in TiO_2 structure for different composition films are proposed.

Acknowledgements The work was supported by ERDF "Institute of Environmental Technology-Excellent Research" (No. CZ.02.1.01/0.0/0.0/16_019/0000853) and by using Large Research Infrastructure ENREGAT supported by the Ministry of Education, Youth and Sports of the Czech Republic under project No. LM2018098. Part of the research presented in this paper was conducted in the Nanomicroscopy Center of the OtaNano research infrastructure in Aalto University. C.T. acknowledges the financial support of the Vilho, Yrjö ja Kalle Väisälä Fund issued by the Finnish Academy of Sciences and Letters. C.T. and I.T. acknowledge the financial support of the Academy of Finland, projects 285972 and 319018, and the Academy of Finland Flagship Programme PREIN (320167).

Compliance with ethical standards

Conflict of interest On behalf of all authors, the corresponding author states that there is no conflict of interest.

References

Ahmed LM, Ivanova I, Hussein FH, Bahnemann DW (2014) Role of platinum deposited on TiO_2 in photocatalytic methanol oxidation and dehydrogenation reactions. Int J Photoenergy. https://doi.org/10.1155/2014/503516

Beranek R, Kisch H (2008) A hybrid semiconductor electrode for wavelength-controlled switching of the photocurrent direction. Angew Chemie Int Ed 47:1320–1322. https://doi.org/10.1002/anie.200701103

Beranek R, Neumann B, Sakthivel S, Janczarek M, Dittrich T, Tributsch H, Kisch H (2007) Exploring the electronic structure of nitrogen-modified TiO_2 photocatalysts through photocurrent and surface photovoltage studies. Chem Phys 339:11–19. https://doi.org/10.1016/j.chemphys.2007.05.022

Bernsmeier D, Sachse R, Bernicke M et al (2019) Outstanding hydrogen evolution performance of supported Pt nanoparticles : Incorporation of preformed colloids into mesoporous carbon films. J Catal 369:181–189. https://doi.org/10.1016/j.jcat.2018.11.006

Choi J, Park H, Hoffmann MR (2010) Effects of single metal-ion doping on the visible-light photoreactivity of TiO_2. J Phys Chem C 114:783–792. https://doi.org/10.1021/jp908088x

Choudhury B, Dey M, Choudhury A (2013) Defect generation, d–d transition, and band gap reduction in Cu-doped TiO_2 nanoparticles. Int Nano Lett. http://www.inl-journal.com/content/3/1/25

Danilovic N, Subbaraman R, Strmcnik D et al (2012) Enhancing the alkaline hydrogen evolution reaction activity through the bifunctionality of Ni $(OH)_2$/metal catalysts. Angew Chem Int Ed 51:12495–12498. https://doi.org/10.1002/anie.201204842

de Richter R, Caillol S (2011) Fighting global warming: the potential of photocatalysis against CO_2, CH_4, N_2O, CFCs, tropospheric O_3, BC and other major contributors to climate change. J Photochem Photobiol C Photochem Rev 12:1–19. https://doi.org/10.1016/j.jphotochemrev.2011.05.002

Di Paola A, Bellardita M, Palmisano L (2013) Brookite, the least known TiO_2photocatalyst. Catalysts 3:36–73. https://doi.org/10.3390/catal3010036

Dolat D, Mozia S, Ohtani B, Morawski AW (2013) Nitrogen, iron-single modified (N–TiO_2, Fe–TiO_2) and Co-modified (Fe, N–TiO_2) rutile titanium dioxide as visible-light active photocatalysts. Chem Eng J 225:358–364. https://doi.org/10.1016/j.cej.2013.03.047

Eftekhari A (2017) Electrocatalysts for hydrogen evolution reaction. Int J Hydrogen Energy 42:11053–11077. https://doi.org/10.1016/j.ijhydene.2017.02.125

Etacheri V, Di C, Schneider J, Bahnemann D, Pillai SC (2015) Photochemistry reviews visible-light activation of TiO_2 photocatalysts: advances in theory and experiments. J Photochem Photobiol C 25:1–29. https://doi.org/10.1016/j.jphotochemrev.2015.08.003

Frindell KL, Bartl MH, Popitsch A, Stucky GD (2002) Sensitized luminescence of trivalent europium by three-dimensionally arranged anatase nanocrystals in mesostructured titania thin films. Angew Chem 114:1001–1004. https://doi.org/10.1002/1521-3757(20020315)114:6%3c1001::AID-ANGE1001%3e3.0.CO;2-8

Fuentes RE, Farell J, Weidner JW (2011) Multimetallic electrocatalysts of Pt, Ru, and Ir supported on anatase and rutile TiO_2 for oxygen evolution in an acid environment. Electrochem Solid State Lett 14:5–7. https://doi.org/10.1149/1.3528163

Gaidai SV, Gryn'ko VS, Zhludenko M, Dyachenko AG, Tkach VM, Ishchenko OV (2017) Activity of carbon-fiber-supported Fe–Co catalysts in the CO_2 methanation reaction. J Superhard Mater 39:122–128. https://doi.org/10.3103/S1063457617020071

García BL, Fuentes R, Weidner JW (2007) Low-temperature synthesis of a PtRu/$Nb_{0.1}Ti_{0.9}O_2$ electrocatalyst for methanol oxidation. Electrochem Solid-State Let 10:108–110. https://doi.org/10.1149/1.2732074

Gnatyuk Y, Smirnova N, Korduban O, Eremenko A (2010) Effect of zirconium incorporation on the stabilization of TiO_2 mesoporous structure. Surf Interface Anal 42:1276–1280. https://doi.org/10.1002/sia.3494

Goncharuk O, Shipul O, Dyachenko A et al (2019) Silica-supported Ni and Co nanooxides: colloidal properties and interactions with polar and nonpolar liquids. J Mol Liq 285:397–402. https://doi.org/10.1016/j.molliq.2019.04.127

Grätzel M, Rotzinger FP (1985) The Influence of the crystal lattice structure on the conduction band energy of oxides of titanium (IV). Chem Phys Lett 118:474–477. https://doi.org/10.1016/0009-2614(85)85335-5

Ihnatiuk DV, Smirnova NP, Linnik OP (2017) Nonporous platinum doped titania films: synthesis, optical and photocatalytic characterization. Chem Phys Technol Surf 8:369–375. https://doi.org/10.15407/hftp08.04.369

Ihnatiuk D, Tossi C, Tittonen I, Linnik O (2020) Effect of synthesis conditions of nitrogen and platinum co-doped titania films on the photocatalytic performance under simulated solar light. Catalysts. https://doi.org/10.3390/catal10091074

Ischenko EV, Yatsimirsky VK, Dyachenko AG, Borysenko MV, Prilutskiy EV, Kongurova IV (2008) Cu-Co-Fe oxide catalysts

supported on carbon nanotubes in the reaction of CO oxidation. Pol J Chem 82:291–297
Ismail AA, Bahnemann DW (2010) Metal-free porphyrin-sensitized mesoporous titania films for visible-light indoor air oxidation. Chemsuschem 3:1057–1062. https://doi.org/10.1002/cssc.201000158
Ismail AA, Kandiel TA, Bahnemann DW (2010) Novel (and better?) titania-based photocatalysts: brookite nanorods and mesoporous structures. J Photochem Photobio A Chem 216:183–193. https://doi.org/10.1016/j.jphotochem.2010.05.016
Khalyavka TA, Shcherban ND, Shymanovska VV, Manuilov EV, Permyakov VV, Shcherbakov SN (2019) Cerium-doped mesoporous $BaTiO_3/TiO_2$ nanocomposites: structural, optical and photocatalytic properties. Res Chem Intermed 45:4029–4042. https://doi.org/10.1007/s11164-019-03888-z
Kisch H (2015) Semiconductor photocatalysis principles and application. Wiley-VCH, Weinheim
Kisch H, Sakthivel S, Janczarek M, Mitoraj D (2007) A low-band gap, nitrogen-modified titania visible-light photocatalyst. J Phys Chem C 111:11445–11449. https://doi.org/10.1021/jp066457y
Kočí K, Krejčíková S, Lacný Z, Šolcová O, Obalová L (2012) Photocatalytic decomposition of N_2O on Ag–TiO_2. Catal Today 191:134–137. https://doi.org/10.1016/j.cattod.2012.01.021
Kočí K, Reli M, Troppová I et al (2017) Photocatalytic decomposition of N_2O over TiO_2/g-C_3N_4 photocatalysts heterojunction. Appl Surf Sci 396:1685–1695. https://doi.org/10.1016/j.apsusc.2016.11.242
Krishna MG, Rao KN, Mohan S (1993) Properties of ion assisted deposited titania films. J Appl Phys 73:434–438. https://doi.org/10.1063/1.353868
Linnik O, Manuilov E, Snegir S, Smirnova N, Eremenko A (2009) Photocatalytic degradation of tetracycline hydrochloride in aqueous solution at ambient conditions stimulated by gold containing zinc-titanium oxide films. J Adv Oxid Technol 12:265–270. https://doi.org/10.1515/jaots-2009-0218
Linnik O, Smirnova N, Korduban O, Eremenko A (2013) Gold nanoparticles into $Ti_{1-x}Zn_xO_2$ films: synthesis, structure and application. Mater Chem Phys 142:318–324. https://doi.org/10.1016/j.matchemphys.2013.07.023
Linnik O, Stefan N, Chorna N et al (2020) Investigation of nitrogen and iron co-doped TiO_2 films synthesized in N_2/CH_4 via pulsed laser deposition technique. Appl Nanosci 10:2569–2579. https://doi.org/10.1007/s13204-020-01309-x
Liu D, Wu Z, Tian F, Ye B-C, Tong Y (2016) Synthesis of N and La co-doped TiO_2/AC photocatalyst by microwave irradiation for the photocatalytic degradation of naphthalene. J Alloys Compd 676:489–498. https://doi.org/10.1016/j.jallcom.2016.03.124
Meng F, Hong Zh, Arndt J et al (2012) Visible light photocatalytic activity of nitrogen-doped $La_2Ti_2O_7$ nanosheets originating from band gap narrowing. Nano Res 5:213–221. https://doi.org/10.1007/s12274-012-0201-x
Meng C, Wang B, Gao Z, Liu Z, Zhang Q, Zhai J (2017) Insight into the role of surface wettability in electrocatalytic hydrogen evolution reactions using light-sensitive nanotubular TiO_2 supported Pt electrodes. Sci Rep. https://doi.org/10.1038/srep41825
Obalova L, Reli M, Ya L et al (2013) Photocatalytic decomposition of nitrous oxide using TiO_2 and Ag–TiO_2 nanocomposite thin films. Catal Today 209:170–175. https://doi.org/10.1016/j.cattod.2012.11.012
Ono LK, Yuan B, Heinrich H, Cuenya BR (2010) Formation and thermal stability of platinum oxides on size-selected platinum nanoparticles: support effects. J Phys Chem C 114:22119–22133. https://doi.org/10.1021/jp1086703
Parson R (1957) The rate of electrocatalytic hydrogen evolution and the heat of adsorption of hydrogen. Trans Faraday Soc 54:1053–1063
Reli M, Kobielusz M, Matějová L et al (2017) TiO_2processed by pressurized hot solvents as a novel photocatalyst for photocatalytic reduction of carbon dioxide. Appl Surf Sci 391:282–287. https://doi.org/10.1016/j.apsusc.2016.06.061
Rothenberger G, Fitzmaurice D, Gratzel M (1992) Spectroscopy of conduction band electrons in transparent metal oxide semiconductor films: optical determination of the flatband potential of colloidal titanium dioxide films. J Phys Chem 96:5983–5986. https://doi.org/10.1021/j100193a062
Sano T, Negishi N, Mas D, Takeuchi K (2000) Photocatalytic decomposition of N_2O on highly dispersed Ag^+ ions on TiO_2 prepared by photodeposition. J Catal 194:71–79. https://doi.org/10.1006/jcat.2000.2915
Serpone N (2006) Is the band gap of pristine TiO_2 narrowed by anion- and cation-doping of titanium dioxide in second-generation photocatalysts? J Phys Chem B 110:24287–24293. https://doi.org/10.1021/jp065659r
Shibata T, Irie H, Ohmori M, Nakajima A, Watanabe T, Hashimoto K (2004) Comparison of photochemical properties of brookite and anatase TiO_2 films. Phys Chem Chem Phys 6:1359–1362. https://doi.org/10.1039/B315777F
Singh AP, Kumari S, Shrivastav R, Dass S, Satsangi VR (2008) Iron doped nanostructured TiO_2 for photoelectrochemical generation of hydrogen. Int J Hydrog Energy 33:5363–5368. https://doi.org/10.1016/j.ijhydene.2008.07.041
Smirnova N, Gnatyuk Yu, Eremenko A et al (2006) Photoelectrochemical characterization and photocatalytic properties of mesoporous TiO_2/ZrO_2 films. Int J Photoenergy. https://doi.org/10.1155/IJP/2006/85469
Smirnova N, Petrik I, Vorobets V, Kolbasov G, Eremenko A (2017) Sol-gel synthesis, photo- and electrocatalytic properties of mesoporous TiO_2 modified with transition metal ions. Nanoscale Res Lett. https://doi.org/10.1186/s11671-017-2002-3
Smirnova N, Petrik I, Linnik O, Eremenko A (2019) Synthesis and photocatalytic properties of 3-d metal ions (Mn Co, Ni, Cu, Fe) doped titania nanostructured films. In: Melnyk IV, Vaclavikova M, Seisenbaeva GA, Kessler VG (eds) Biocompatible hybrid oxide health nanoparticles for human health: from synthesis to applications. Elsevier, Amsterdam, pp 67–82
Subbaraman R, Tripkovic D, Strmcnik D et al (2011) Enhancing hydrogen evolution activity in water splitting by tailoring Li^+-$Ni(OH)_2$-Pt interfaces. Science 334:1256–1260. https://doi.org/10.1126/science.1211934
Tossi C, Hällström L, Selin J, Vaelma M, See E, Lahtinen J, Tittonen I (2019) Size- and density-controlled photodeposition of metallic platinum nanoparticles on titanium dioxide for photocatalytic applications. J Mater Chem A 7:14519–14525. https://doi.org/10.1039/C8TA09037H
Wang R, Hashimoto K, Fujishima A et al (1998) Photogeneration of highly amphiphilic TiO_2 surfaces. Adv Mater 10:135–138. https://doi.org/10.1002/(SICI)1521-4095(199801)10:2%3c135::AID-ADMA135%3e3.0.CO;2-M
Yi L, Zhang H, Xu T, Lu Z, Wu X, Wan P (2015) Under-water superaerophobic pine-shaped Pt nanoarray electrode for ultrahigh-performance hydrogen evolution. Adv Funct Mater 25:1737–1744. https://doi.org/10.1002/adfm.201404250
Yi W, Shin C-H, Tetteh EB, Lee B-J, Yu J-S (2020) Insight into the boosted electrocatalytic oxygen evolution performance of highly hydrophilic nickel–iron hydroxide. ACS Appl Energy Mater 3:822–830. https://doi.org/10.1021/acsaem.9b01952
Yu F-Y, Lang Z-L, Yin L-Y (2020) Pt–O bond as an active site superior to Pt^0 in hydrogen evolution reaction. Nat Commun. https://doi.org/10.1038/s41467-019-14274-z